


Article

Active Fault-Tolerant Cooperative Control for Multi-QUAVs Using Relative Measurement Information

Yujiang Zhong¹ , Xi Chen¹, Ping Li¹, Pinfan Hou², Zhen Wang^{1,*} and Kunlin Nie^{3,4}¹ School of Cybersecurity, Northwestern Polytechnical University, Xi'an 710072, China; yujiangzhong@hotmail.com (Y.Z.); cenxisz@163.com (X.C.)² School of Aeronautics, Northwestern Polytechnical University, Xi'an 710072, China; houpinfan@mail.nwpu.edu.cn³ National Elite Institute of Engineering, Northwestern Polytechnical University, Xi'an 710072, China; niekl@mail.nwpu.edu.cn⁴ Ancyber, Beijing 100144, China

* Correspondence: w-zhen@nwpu.edu.cn

Highlights

What are the main findings?

- A decoupled fault estimation observer is developed based on the derived observable subsystem, capable of estimating actuator faults and the leader's unknown input signal.
- An active fault-tolerant cooperative control method is proposed, ensuring consensus-based formation stability for multi-QUAV systems with relative output measurements.

What is the implication of the main finding?

- Actuator fault can be estimated using relative output measurements, which is a challenge for multi-QUAVs due to the coupling of relative measurement information.
- The fault-tolerant method allows consensus-based formation control using only relative outputs, eliminating leader dependency and the need for absolute measurements.

Abstract

This paper investigates actuator fault-tolerant cooperative control of multiple quadrotor unmanned aerial vehicles (multi-QUAVs) under restricted communication conditions, where only relative output measurements are available. By appropriately transforming and scaling the control inputs and outputs of the multi-QUAVs, an observable subsystem is constructed. A decoupled fault estimation observer is then designed for this subsystem to estimate actuator faults and the leader's input signal. Based on the fault estimation information and relative measurement information among QUAVs, a node-based active fault-tolerant cooperative control law is developed. This approach enables multi-QUAVs to achieve consensus-based formation solely relying on relative output information, even in the presence of actuator faults. Finally, the effectiveness of the proposed active fault-tolerant cooperative control method is verified by simulation.

Keywords: multi-QUAVs; actuator faults; relative output measurements; decoupled fault estimation observer; active fault-tolerant cooperative control



Academic Editor: Bo Li

Received: 31 July 2025

Revised: 30 September 2025

Accepted: 5 October 2025

Published: 11 October 2025

Citation: Zhong, Y.; Chen, X.; Li, P.; Hou, P.; Wang, Z.; Nie, K. Active Fault-Tolerant Cooperative Control for Multi-QUAVs Using Relative Measurement Information. *Drones* **2025**, *9*, 699. <https://doi.org/10.3390/drones9100699>

Copyright: © 2025 by the authors.

Licensee MDPI, Basel, Switzerland.

This article is an open access article distributed under the terms and

conditions of the Creative Commons Attribution (CC BY) license

(<https://creativecommons.org/licenses/by/4.0/>).

1. Introduction

With benefits like improved reliability, cost efficiency, and adaptable configurations, multiple quadrotor unmanned aerial vehicles (multi-QUAVs) have gained significant interest from various scientific communities in recent decades and are widely employed

in civilian projects and military operations [1–5]. Multi-QUAVs can be comprehended as a series of interactive QUAVs in an interconnected network, collaboratively maintaining a formation via common cooperative control laws [6–8]. Due to the strong nonlinearity and underactuated characteristics of the quadrotor unmanned aerial vehicle (QUAV), it is a great challenge to design a cooperative control scheme to accurately achieve the expected formation shape for multi-QUAVs [9,10].

During the past few decades, consensus-based control for multi-QUAVs has undergone substantial advancements. Reference [11] proposes a consensus–inference-based hierarchical reinforcement learning scheme to address multi-constrained unmanned aerial vehicle (UAV) pursuit–evasion game challenges. To achieve optimal active fault-tolerant bipartite consensus control in UAV swarms subject to nonidentical and unknown direction faults and disturbances, reference [12] proposes a switching function-based fault-tolerant control (FTC) framework. This framework integrates reinforcement learning-optimized control, distributed observer design, and active fault detection mechanisms. Xiao in [13] introduces a distributed fixed-time group consensus control method to tackle uncertain disturbances and enhance reliability and efficiency during inspection tasks for multi-UAVs. A distributed fixed-time group consensus control scheme for multi-UAVs under disturbances is developed in [14]. This scheme uses radial basis function neural networks to estimate uncertainties and a backstepping approach with command filters to ensure the fixed-time convergence of consensus errors.

In a networked multi-QUAV system, a single fault on a QUAV probably induces drastic cascading failures through inter-agent coupling effects and compromises global formation stability and mission safety [15]. Therefore, to address the aforementioned challenges, significant advances have been made in recent years in fault-tolerant control, particularly in passive fault-tolerant control approaches. In [16], Guo proposes a dynamic event-triggered predefined-time adaptive sliding mode control scheme to address fault-tolerant control to address the actuator faults in the attitude tracking of a UAV. For the faults in formation tracking–containment control of UAVs, Hu in [17] proposes a differential game-based approach integrated with adaptive dynamic programming to solve the challenges of fault-tolerant coordination. A passive fault-tolerant control strategy is proposed in [18] for the transition flight phase of dual-system UAVs. A two-step robust fault-tolerant controller is designed in [19] for the complex and nonlinear dynamics of UAVs to address disturbances and actuator faults. Reference [20] designs an adaptive event-triggered finite-time fault-tolerant containment control scheme for multi-UAVs subject to input constraints, actuator failures, communication limitations, and external disturbances.

The control design methods mentioned above are all based on the passive fault-tolerant control framework. However, in some critical scenarios, UAVs require immediate reaction to faults and rapid compensation to prevent failure propagation throughout other UAVs. To address this demanding requirement, active fault-tolerant control is proposed as a solution. For the vortex effects under simultaneous actuator and sensor faults in a heterogeneous multi-UAV system, reference [21] develops an observer-based fault-tolerant control integrating decentralized fault estimation and FTC mechanisms. A dual-loop active fault-tolerant controller for UAV formations is proposed in [22], where an outer loop controller and an inner loop controller stabilize the system and ensure accurate tracking of desired trajectories, respectively. Yang [23] introduces a backstepping-based fault-tolerant cooperative control strategy for multi-fixed-wing UAVs under the actuator faults, with sensor faults via wind disturbances; this approach incorporates adaptive fault detection thresholds and a backstepping-based fault-tolerant control scheme to enhance robustness under dynamic uncertainties. In [24], a novel distributed intermediate estimator-based fault-tolerant tracking protocol is proposed to address the problem of multi-agent systems with

multiple faults and mismatched disturbances. In [25], a fault-tolerant control algorithm based on sliding mode and an adaptive control strategy is proposed for UAV surface structural damage. Developments in motor failures on the UAV have been discussed by Abdullah in [26], who proposes a nonlinear disturbance observer-based sliding mode control for rotational motion control. Reference [27] proposes a sliding-mode-based fault diagnosis and fault-tolerant control method for quadrotor trajectory tracking under actuator faults and external disturbances. For actuator faults with unknown reference signals, Amador-Macias [28] designs a high-gain observer-based fault-tolerant control approach.

However, active fault-tolerant cooperative control (AFTCC) strategies for multi-QUAVs remain under-explored, especially with the communication-constrained conditions. When the relative measurements obtained by onboard measurement devices are available, an effective AFTCC scheme is particularly challenging. For this reason, this paper will develop an AFTCC method for multi-QUAVs based on relative output information. The key innovations of this paper can be summarized as follows:

1. This paper conducts research on consensus-based formation control for multi-QUAVs with the relative measurements. An active fault-tolerant cooperative control framework against actuator faults is proposed, which consists of a decoupled fault estimation observer and an active fault-tolerant cooperative control law.
2. Within the fault estimation observer design for the decoupled relative QUAV system, incorporating a proportional-integral mechanism ensures quick detection of time-varying faults and reproduces the magnitudes of the fault. The convergence of this proposed decoupled fault estimation observer is proven via linear matrix inequality (LMI) constraints and exhibits H_∞ performance.
3. An active fault-tolerant cooperative control law is proposed to handle actuator faults. The AFTCC method quickly compensates for the time-varying faults and prevents fault propagation within the multi-QUAVs formation system, thereby enhancing the robustness of the multi-QUAV system.

2. Preliminaries

2.1. Graph Theory

A multi-QUAV system is composed of N QUAV, and the interaction of the multi-QUAVs can be described by an undirected graph $\mathcal{G} = (\mathcal{V}, \mathcal{E})$, where $\mathcal{V} = \{v_i | i = 1, \dots, N\}$ and $\mathcal{E} \subseteq \mathcal{V} \times \mathcal{V}$ denote the node set and edge set, respectively. The adjacent matrix of \mathcal{G} is $\mathcal{A} = [a_{ij}] \in \mathbb{R}^{N \times N}$ and $a_{ij} = 0$, if $(v_i, v_j) \notin \mathcal{E}$; $a_{ij} = 1$, otherwise. $a_{ij} = 1$ indicates that the i -th QUAV can receive information from the j -th QUAV, and \mathcal{N}_i is the set of all neighboring nodes. The degree of the i -th node is $d_i = \sum_{j=1}^N a_{ij}$ and the degree matrix $\mathcal{D} = \text{diag}(d_1, d_2, \dots, d_N)$. The Laplacian matrix of the graph \mathcal{G} is defined as follows:

$$\mathcal{L}_{ij} = \begin{cases} d_i & \text{if } i = j, \\ -a_{ij} & \text{if } i \neq j. \end{cases}$$

Lemma 1 ([29]). *For a connected undirected graph \mathcal{G} , the symmetric matrix \mathcal{L} is rank deficient and the eigenvalues of \mathcal{L} can be written as $\lambda_N > \lambda_{N-1} > \dots > \lambda_2 > \lambda_1 = 0$. Furthermore, there exists an orthogonal matrix N such that $N^T \mathcal{L} N = \text{diag}(\lambda_N, \dots, \lambda_2, \lambda_1)$.*

2.2. H_∞ Theory

In robust control theory, the H_∞ norm of a multiple-input multiple-output (MIMO) system with transfer function matrix $G(s)$ is defined as the peak of the maximum singular value of the frequency response [30], i.e., $\|G(s)\|_{H_\infty} = \sup_{\omega \in \mathbb{R}} \bar{\sigma}(G(j\omega))$. For a linear time-invariant (LTI) system, the infinity-norm of this system can be equivalently defined as the in-

duced \mathcal{L}_2 -gain and proven via Parseval's identity in [31], i.e., $\|G(s)\|_{H_\infty} = \sup_{\omega(t) \neq 0} \frac{\|z(t)\|_2}{\|\omega(t)\|_2}$, where $\omega(t)$ is the exogenous input signal and $z(t)$ is the regulated output signal. The \mathcal{L}_2 -gain of a MIMO system is defined as the supremum of the ratio between the system input-output's \mathcal{L}_2 norm. The \mathcal{L}_2 norm of any signal $f(t)$ can be calculated as follows:

$$\|f(t)\|_2 = \sqrt{\int_0^\infty f^T(t)f(t)dt} \quad (1)$$

Lemma 2 ([32]). *The LTI system is asymptotically stable and converges with a stability margin exponent $\alpha > 0$ if and only if there exists a matrix $X \in \mathbb{R}^{n \times n}$ such that*

$$A^T X + X^T A + 2\alpha X < 0$$

Lemma 3 ([33]). *For a given symmetric matrix $\Omega = \begin{bmatrix} P & Q \\ Q^T & R \end{bmatrix}$, the following conditions are equivalent:*

- i. $\Omega < 0$.
- ii. $R < 0$ and $P - QR^{-1}Q < 0$.

3. Active Fault-Tolerant Cooperative Control Scheme Design

3.1. Observable Relative Multi-QUAV System

This section mainly considers leader-following multi-QUAVs where communication is strictly limited and only relative measurements are accessible. Based on the aforementioned context, this subsection will conduct linearization of QUAV and establish an observable model for a multi-QUAV system.

3.1.1. Linearizing Quadrotor UAV Model

The QUAV has a simple geometric structure as shown in Figure 1, with four motors symmetrically distributed around the fuselage. To balance the torques, the adjacent motors rotate in opposite directions to generate thrust. Furthermore, the inertial frame and the body frame are defined to describe the motion of a 6-DOF rigid body.

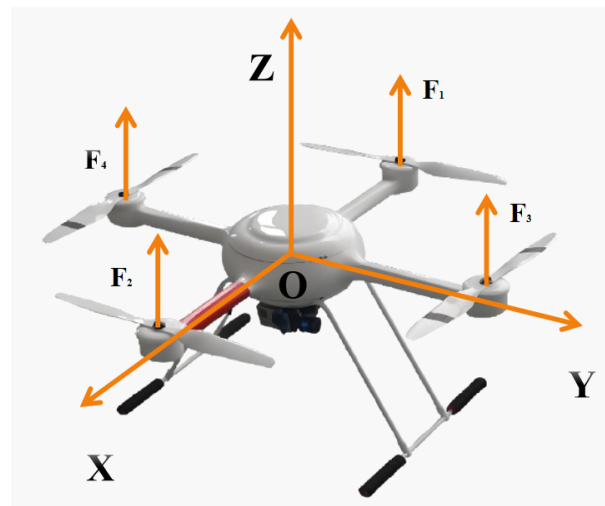


Figure 1. Structure of the Quadrotor UAV.

The dynamics of QUAV have been explored by many researchers as described in [34]. For a multi-QUAV system with $N + 1$ QUAVs, the dynamic model of the i -th QUAV can be expressed as follows:

$$\begin{cases} \ddot{x}_i = (\cos \phi_i \sin \theta_i \cos \psi_i + \sin \phi_i \sin \psi_i) \frac{U_{1,i}}{m} - \frac{k_{dx} \dot{x}_i}{m}, \\ \ddot{y}_i = (\cos \phi_i \sin \theta_i \sin \psi_i - \sin \phi_i \cos \psi_i) \frac{U_{1,i}}{m} - \frac{k_{dy} \dot{y}_i}{m}, \\ \ddot{z}_i = \cos \phi_i \cos \theta_i \frac{U_{1,i}}{m} - \frac{k_{dz} \dot{z}_i}{m} - g, \\ \ddot{\phi}_i = \dot{\theta}_i \psi_i \frac{(I_y - I_x)}{I_x} + \frac{U_{2,i}}{I_x} - Lk_\phi \frac{\dot{\phi}_i}{I_x}, \\ \ddot{\theta}_i = \dot{\phi}_i \psi_i \frac{(I_z - I_x)}{I_y} + \frac{U_{3,i}}{I_y} - Lk_\theta \frac{\dot{\theta}_i}{I_y}, \\ \ddot{\psi}_i = \dot{\theta}_i \phi_i \frac{(I_x - I_y)}{I_z} + \frac{U_{4,i}}{I_z} - Lk_\psi \frac{\dot{\psi}_i}{I_z}. \end{cases} \quad (2)$$

where coordinates (x_i, y_i, z_i) and $(\phi_i, \theta_i, \psi_i)$ represent the position and the Euler angles of roll, pitch, and yaw of i -th QUAV, respectively; m is the mass of QUAV, g denotes the gravitational acceleration, L is the distance between the mass center of QUAV and the center of the rotor, and $k_{dx}, k_{dy}, k_{dz}, k_\phi, k_\theta, k_\psi$ are the drag coefficients in and around three directions, respectively; I_x, I_y, I_z are the moments of inertia along three axes, respectively.

The inputs $U_{1,i}, U_{2,i}, U_{3,i}, U_{4,i}$ are the i -th QUAV's total lift force and moments about the roll, pitch, and yaw axes, respectively. The system inputs of the i -th QUAV are as follows:

$$\begin{cases} U_{1,i} = F_{1,i} + F_{2,i} + F_{3,i} + F_{4,i}, \\ U_{2,i} = L(F_{3,i} - F_{4,i}), \\ U_{3,i} = L(F_{1,i} - F_{2,i}), \\ U_{4,i} = K_y(F_{1,i} + F_{2,i} - F_{3,i} - F_{4,i}). \end{cases} \quad (3)$$

where K_y is the thrust-to-moment scaling factor, and $F_{1,i}, F_{2,i}, F_{3,i}, F_{4,i}$ denote the individual thrusts generated by the four rotors of the i -th QUAV.

Assumption 1. The multi-QUAV system operates in hovering mode ($U_{1,i} \approx mg$) and executes slow translational and rotational motions such that all drag force can be neglected, and the ϕ, θ, ψ angles of each QUAV are small such that all Euler angles and their time derivatives are approximately zero.

Based on Assumption 1, the nonlinear dynamic model of the i -th QUAV can be simplified into a linear time-invariant system as follows:

$$\begin{cases} \ddot{x}_i = \theta g, \\ \ddot{y}_i = -\phi g, \\ \ddot{z}_i = \frac{U_{1,i}}{m} - g, \\ \ddot{\phi}_i = \frac{U_{2,i}}{I_x}, \\ \ddot{\theta}_i = \frac{U_{3,i}}{I_y}, \\ \ddot{\psi}_i = \frac{U_{4,i}}{I_z}. \end{cases} \quad (4)$$

The MIMO state-space form of the linearized dynamic system of a QUAV can be written as follows:

$$\begin{cases} \dot{\xi}_i(t) = A\xi_i(t) + Bu_i(t) + G_g g, \\ z_i(t) = \sum_{j \in \mathcal{N}_i} C(\xi_i(t) - \xi_j(t)). \end{cases} \quad (5)$$

where ξ_i denotes $[x_i \dot{x}_i y_i \dot{y}_i z_i \dot{z}_i \phi_i \dot{\phi}_i \theta_i \dot{\theta}_i \psi_i \dot{\psi}_i]^T \in \mathbb{R}^{12 \times 1}$, u_i represents $[F_{1,i} F_{2,i} F_{3,i} F_{4,i}]^T \in \mathbb{R}^{4 \times 1}$, and $\mathcal{N}_i \subset \{0, 1, 2, \dots, N\} \setminus \{i\}$ is the QAVs with which the i -th QAV interacts. $z_i(t) \in \mathbb{R}^{p \times 1}$ is the sum of relative measurements of the i -th QAV. The matrices A , B , and G_g can be defined as follows:

$$A = \begin{bmatrix} 0 & 1 & 0 & 0 & 0 & 0 & 0 & 0 & 0 & 0 & 0 & 0 \\ 0 & 0 & 0 & 0 & 0 & 0 & 0 & 0 & g & 0 & 0 & 0 \\ 0 & 0 & 0 & 1 & 0 & 0 & 0 & 0 & 0 & 0 & 0 & 0 \\ 0 & 0 & 0 & 0 & 0 & 0 & -g & 0 & 0 & 0 & 0 & 0 \\ 0 & 0 & 0 & 0 & 0 & 1 & 0 & 0 & 0 & 0 & 0 & 0 \\ 0 & 0 & 0 & 0 & 0 & 0 & 0 & 0 & 0 & 0 & 0 & 0 \\ 0 & 0 & 0 & 0 & 0 & 0 & 0 & 1 & 0 & 0 & 0 & 0 \\ 0 & 0 & 0 & 0 & 0 & 0 & 0 & 0 & 0 & 0 & 0 & 0 \\ 0 & 0 & 0 & 0 & 0 & 0 & 0 & 0 & 0 & 1 & 0 & 0 \\ 0 & 0 & 0 & 0 & 0 & 0 & 0 & 0 & 0 & 0 & 0 & 0 \\ 0 & 0 & 0 & 0 & 0 & 0 & 0 & 0 & 0 & 0 & 0 & 1 \\ 0 & 0 & 0 & 0 & 0 & 0 & 0 & 0 & 0 & 0 & 0 & 0 \end{bmatrix}, B = \begin{bmatrix} 0 & 0 & 0 & 0 \\ 0 & 0 & 0 & 0 \\ 0 & 0 & 0 & 0 \\ 0 & 0 & 0 & 0 \\ 0 & 0 & 0 & 0 \\ \frac{1}{m} & \frac{1}{m} & \frac{1}{m} & \frac{1}{m} \\ 0 & 0 & 0 & 0 \\ 0 & 0 & \frac{L}{I_x} & -\frac{L}{I_x} \\ 0 & 0 & 0 & 0 \\ \frac{L}{I_y} & -\frac{L}{I_y} & 0 & 0 \\ 0 & 0 & 0 & 0 \\ \frac{K_y}{I_z} & \frac{K_y}{I_z} & -\frac{K_y}{I_z} & -\frac{K_y}{I_z} \end{bmatrix}, G_g = \begin{bmatrix} 0 \\ 0 \\ 0 \\ 1 \\ 0 \\ 0 \\ 0 \\ 0 \\ 0 \\ 0 \\ 0 \\ 0 \end{bmatrix}$$

During the actual flight mission, the system may experience both time-varying faults and external disturbances due to motors overheating, leading to aging and other unexpected physical parameters. Therefore, the dynamic model of the i -th QAV with external disturbances and actuator faults can be written as follows:

$$\begin{cases} \dot{\xi}_i(t) = A\xi_i(t) + Bu_i(t) + Dd_i(t) + Ef_i(t) + G_g g, \\ z_i(t) = \sum_{j \in \mathcal{N}_i} C(\xi_i(t) - \xi_j(t)). \end{cases} \quad (6)$$

where $d_i(t) \in \mathbb{R}^{d \times 1}$ and $f_i(t) \in \mathbb{R}^{r \times 1}$ are the disturbance signal and fault signal, respectively. Moreover, the external disturbance signal and time-varying fault signal are bounded, i.e., $\|f_i(t)\| < \beta_f$, $\|u_i(t)\| < \beta_u$ for $i = 1, 2, \dots, N$, where β_f and β_u are positive known constants. The matrix are $C \in \mathbb{R}^{p \times 12}$, $D \in \mathbb{R}^{12 \times d}$, and $E \in \mathbb{R}^{12 \times r}$.

3.1.2. Observable Subsystem of the Multi-QUAV System

The aim of this paper is to design an AFTCC law for a leader-following multi-QUAV system using the relative measurements, with the primary objective of maintaining collaborative stability. The multi-QUAVs operate under communication bandwidth limitations, in which only relative output information is accessible to each QAV. Consequently, a collection of $N + 1$ QAVs is considered as a total system. For that purpose, the following assumptions are needed.

Assumption 2. The communication topology between the leader and followers is limited and unidirectional, but the information exchange among followers is bidirectional. Furthermore, the leader QAV is fault-free throughout the flight such that $f_0(t) \equiv 0$, and the dynamic model can be defined as follows:

$$\begin{cases} \dot{\xi}_0(t) = A\xi_0(t) + Bu_0(t) + Dd_0(t) + G_g g, \\ y_0(t) = C\xi_0. \end{cases} \quad (7)$$

Assumption 3. The control input matrix B and fault distribution matrix E satisfy $\text{rank}([B \ E]) = \text{rank}(B)$, implying that $(I_n - BB^\dagger)E = 0$, i.e., the effect of actuator faults belongs to the actuation space $\text{Im}(B)$.

The overall multi-QUAV system is given as follows:

$$\begin{cases} \dot{\xi}(t) = (I_{N+1} \otimes A)\xi(t) + (I_{N+1} \otimes B)u(t) + (I_{N+1} \otimes D)d(t) + (I_{N+1} \otimes E)f(t) + (I_N \otimes G_g)g, \\ z(t) = (\mathcal{L} \otimes C)\xi(t). \end{cases} \quad (8)$$

where $\xi(t) = [\xi_0(t), \xi_1(t), \dots, \xi_N(t)]^T$, $u(t) = [u_0(t), \dots, u_N(t)]^T$, $d(t) = [d_0(t), \dots, d_N(t)]^T$, $f(t) = [0, f_1(t), \dots, f_N(t)]^T$, and $z(t) = [z_0(t), z_1(t), \dots, z_N(t)]^T$.

According to [35], the observability matrix of system (8) has a non-zero null space, so certain subspaces in the state vector are not observable. To extract an observable subspace, define a coordinate transformation $\xi \rightarrow T_1 \xi = \xi'$, where $T_1 = N^{-1} \otimes I_n$. Let N be a nonsingular matrix:

$$N^{-1} = \begin{bmatrix} 1 & \mathbf{0}_N \\ -\mathbf{1}_N & \mathbf{I}_N \end{bmatrix}$$

where $\mathbf{1}_N \in \mathbb{R}^{N \times 1}$ is all non-negative ones, and each element of $\mathbf{0}_N \in \mathbb{R}^{1 \times N}$ is zero.

Applying the transformation T_1 to the state vector:

$$\xi'(t) = \text{Col}(\xi_0(t), \bar{\xi}(t)) = [\xi_0^T(t), \bar{\xi}_1^T(t), \dots, \bar{\xi}_N^T(t)] \quad (9)$$

where $\bar{\xi}_i(t) = \xi_i(t) - \xi_0(t)$, for $i \in 1, 2, \dots, N$, and $\bar{\xi}(t) = (\bar{\xi}_1^T(t), \dots, \bar{\xi}_2^T(t), \dots, \bar{\xi}_N^T(t))$. The transformation $(A, B, C, D, E) \rightarrow (\bar{A}, \bar{B}, \bar{C}, \bar{D}, \bar{E})$ is defined, where

$$\begin{cases} A_1 = T_1(I_{N+1} \otimes A)T_1^{-1} = (I_N \otimes A), \\ B_1 = T_1(I_{N+1} \otimes B) = (N^{-1} \otimes B) = (I_N \otimes B)(N^{-1} \otimes I_m), \\ D_1 = T_1(I_{N+1} \otimes D) = (N^{-1} \otimes D) = (I_N \otimes D)(N^{-1} \otimes I_d), \\ E_1 = T_1(I_{N+1} \otimes E) = (N^{-1} \otimes E) = (I_N \otimes E)(N^{-1} \otimes I_r), \\ G_{g1} = T_1(I_{N+1} \otimes G_g) = (N^{-1} \otimes G_g) = (I_N \otimes G_g)(N^{-1} \otimes I_{12}), \\ C_1 = (\mathcal{L} \otimes C)T_1^{-1} = (\mathcal{L} \otimes C)(N \otimes I_n) = (\mathcal{L}N \otimes C). \end{cases} \quad (10)$$

This transformation T_1 yields a new system representation.

$$\begin{cases} \dot{\xi}'(t) = A_1 \xi'(t) + B_1 u(t) + D_1 d(t) + E_1 f(t) + G_{g1} g, \\ z'(t) = C_1 \xi'(t). \end{cases} \quad (11)$$

To decouple the relative sensing signal, define the scaling transformation $Z_1 = (N^T \otimes I_p)$ on the vector $z_0(t)$ to create the following:

$$z_0(t) = (N^T \otimes I_p)z'(t) = (N^T \otimes I_p)(\mathcal{L}N \otimes C)\xi'(t) = (N^T \mathcal{L}N \otimes C)\xi'(t) \quad (12)$$

Based on Assumption 2 and the row-sum-equal-to-zero property of the Laplacian matrix \mathcal{L} , it can be checked easily:

$$N^T \mathcal{L}N = \begin{bmatrix} 0 & q_{1 \times N} \\ 0_{N \times 1} & \tilde{L} \end{bmatrix} \quad (13)$$

where the upper-left element is the constant 0 due to the row-sum-equal-to-zero property of \mathcal{L} , and $q_{1 \times N}$ is an appropriate vector. $\tilde{L} \in \mathbb{R}^{N \times N}$ is a submatrix of the Laplacian matrix \mathcal{L} obtained by setting the first column and row to zero.

The scaled relative output measurements in the new coordinate system are

$$z_1(t) = \left(\begin{bmatrix} 0 & q_{1 \times N} \\ 0_{N \times 1} & \tilde{L} \end{bmatrix} \otimes C \right) \begin{bmatrix} \xi_0(t) \\ \bar{\xi}(t) \end{bmatrix} \quad (14)$$

From the definition (10), one has the following:

$$\left\{ \begin{array}{l} B_1 u(t) = (I_{N+1} \otimes B)(N^{-1} \otimes I_m)u(t) = (I_{N+1} \otimes B) \underbrace{\text{Col}(u_0(t), \bar{u}(t))}_{u'}, \\ D_1 d(t) = (I_{N+1} \otimes D)(N^{-1} \otimes I_d)d(t) = (I_{N+1} \otimes D) \underbrace{\text{Col}(d_0(t), \bar{d}(t))}_{d'}, \\ E_1 f(t) = (I_{N+1} \otimes E)(N^{-1} \otimes I_r)f(t) = (I_{N+1} \otimes E) \underbrace{\text{Col}(f_0(t), \bar{f}(t))}_{f'}, \\ G_g g = (I_{N+1} \otimes G_g)(N^{-1} \otimes I_{12})g = (I_{N+1} \otimes G_g) \underbrace{\text{Col}(g, 0, \dots, 0)}_N. \end{array} \right. \quad (15)$$

The observable subsystem can be extracted from system (11) by considering the last $N \times n$ rows of the partitioned structure of ζ' , u , and z' , and the observable subsystem can be defined as follows:

$$\left\{ \begin{array}{l} \dot{\bar{\zeta}}(t) = (I_N \otimes A)\bar{\zeta}(t) + (I_N \otimes B)\bar{u}(t) + (I_N \otimes D)\bar{d}(t) + (I_N \otimes E)\bar{f}(t) \\ \bar{z}(t) = (\tilde{L} \otimes C)\bar{\zeta}(t) \end{array} \right. \quad (16)$$

Let $Z_2 = (\tilde{L}^{-1} \otimes I_p)$, and scale $\bar{z}(t)$ by using Z_2 to create the following:

$$\tilde{z}(t) = (\tilde{L}^{-1} \otimes I_p)\bar{z}(t) = (\tilde{L}^{-1} \otimes I_p)(\tilde{L} \otimes C)\bar{x}(t) = (I_N \otimes C)\bar{x}(t) \quad (17)$$

Thus, the decoupled system of the i -th QUAV can be written as follows:

$$\left\{ \begin{array}{l} \dot{\tilde{\zeta}}_i(t) = A\tilde{\zeta}_i(t) + B\bar{u}_i(t) + D\bar{d}_i(t) + E\bar{f}_i(t) \\ \tilde{z}_i = C\tilde{\zeta}_i(t) \end{array} \right. \quad (18)$$

for $i = 1, 2, \dots, N$.

3.2. Relative-Output-Based Fault Estimation Observer

After using transformation and scaling, the decoupled dynamic system (18) can be used as a basis for the design of adaptive observers for reconstruction of the time-varying fault signal $f_i(t)$.

Define $f_{u,i}(t) = B^\dagger E f_i(t) - u_0(t)$, and the system (18) can be written as follows:

$$\dot{\tilde{\zeta}}_i(t) = A\tilde{\zeta}_i(t) + Bu_i(t) + D\bar{d}_i(t) + Bf_{u,i}(t)$$

The following observer is designed.

$$\left\{ \begin{array}{l} \dot{\hat{\zeta}}_i(t) = A\hat{\zeta}_i(t) + Bu_i(t) + B\hat{f}_{u,i}(t) - G(\hat{z}_i(t) - \tilde{z}_i(t)), \\ \hat{z}_i(t) = C\hat{\zeta}_i(t), \\ \dot{\hat{f}}_{u,i}(t) = \hat{f}_{u,i}(t) + S(\hat{z}_i(t) - \tilde{z}_i(t)) + R(\dot{\hat{z}}_i(t) - \dot{\tilde{z}}_i(t)). \end{array} \right. \quad (19)$$

where $\hat{\zeta}_i(t) \in \mathbb{R}^{12 \times 1}$, $\hat{z}_i(t) \in \mathbb{R}^{p \times 1}$, and $\hat{f}_i(t) \in \mathbb{R}^{r \times 1}$ are state estimation, external measurement estimation, and time-varying fault estimation of the i -th QUAV with integration of the leader's control input, respectively. $G \in \mathbb{R}^{12 \times p}$ is the gain matrix of the state estimation equation, and $S \in \mathbb{R}^{r \times p}$ and $R \in \mathbb{R}^{r \times p}$ are the gain matrices of the fault estimation equation.

Let the state estimation error vector $e_{x,i} = \hat{\xi}_i(t) - \tilde{\xi}_i(t)$, the relative outputs error vector $e_{z,i} = \hat{z}_i(t) - \tilde{z}_i(t)$, and fault estimation error vector $e_{f,i} = \hat{f}_{u,i}(t) - f_{u,i}(t)$, where $\hat{f}_{u,i}(t) = B^+ E \hat{f}_i(t) - \hat{u}_0(t)$, one has

$$\begin{aligned}\dot{e}_{x,i}(t) &= \dot{\hat{\xi}}_i(t) - \dot{\tilde{\xi}}_i(t) \\ &= A\hat{\xi}_i(t) + Bu_i(t) + B\hat{f}_{u,i}(t) - G(\hat{z}_i(t) - \tilde{z}_i(t)) \\ &\quad - (A\tilde{\xi}_i(t) + Bu_i(t) + D\tilde{d}_i(t) + B\tilde{f}_{u,i}(t)) \\ &= Ae_{x,i}(t) + Be_{f,i}(t) - D\tilde{d}_i(t)\end{aligned}\quad (20)$$

and

$$\begin{aligned}\dot{e}_{f,i}(t) &= \dot{\hat{f}}_{u,i}(t) - \dot{f}_{u,i}(t) \\ &= \hat{f}_{u,i}(t) + SCe_{x,i}(t) + RC\dot{e}_{x,i}(t) - \dot{f}_{u,i}(t) + \dot{f}_{u,i}(t) - \dot{f}_{u,i}(t) \\ &= (SC + RCA + RCGC)e_{x,i}(t) + (RCE + I_r)e_{f,i}(t) - RCD\tilde{d}_i(t) + f_{u,i}(t) - \dot{f}_{u,i}(t)\end{aligned}\quad (21)$$

By combining Equations (20) and (21), the error dynamics of the augmented system can be derived as follows:

$$\dot{e}_i(t) = (\hat{A} + \hat{G}\hat{C} + \hat{R}\hat{C}\hat{A})e_i(t) + [\hat{I}\hat{R}\hat{C}\hat{D} + \hat{D}]\omega_i(t) \quad (22)$$

$$\text{where } \hat{A} = \begin{bmatrix} A & E \\ 0_{r \times 12} & I_r \end{bmatrix}, \hat{G} = \begin{bmatrix} -G \\ S - RCG \end{bmatrix}, \hat{R} = \begin{bmatrix} 0_{12 \times p} \\ R \end{bmatrix}, \hat{C} = [C \quad 0_{p \times r}], \hat{D} = \begin{bmatrix} -D \\ 0_{r \times d} \end{bmatrix},$$

$$\hat{I} = \begin{bmatrix} 0_{12 \times r} & 0_{12 \times r} \\ I_r & -I_r \end{bmatrix}, e_i = \begin{bmatrix} e_{x,i}(t) \\ e_{f,i}(t) \end{bmatrix}, \text{ and } \omega_i = \begin{bmatrix} f_{u,i}(t) \\ \dot{f}_{u,i}(t) \\ \tilde{d}_i(t) \end{bmatrix}.$$

Theorem 1. The fault estimation observer (22) is asymptotically stable and converges with a stability margin exponent $\alpha > 0$ with H_∞ performance of γ if and only if there exists a positive definite symmetric matrix P such that the following LMI holds:

$$\Omega = \begin{bmatrix} \Omega_{11} & P\hat{I} & \Omega_{13} & I_{12+r} \\ * & -\gamma I_{2r} & 0 & 0 \\ * & * & -\gamma I_d & 0 \\ * & * & * & -\gamma I_{12+r} \end{bmatrix} < 0 \quad (23)$$

$$\Omega_{11} + 2\alpha P < 0 \quad (24)$$

where $\Omega_{11} = P\hat{A} + \hat{A}^T P + Q_1\hat{C} + \hat{C}^T Q_1 + Q_2\hat{C}\hat{A} + \hat{A}^T \hat{C}^T Q_2$, $\Omega_{13} = Q_2\hat{C}\hat{D} + P\hat{D}$, where $Q_1, Q_2 \in \mathbb{R}^{(12+r) \times p}$, and $*$ denotes the symmetric item in a symmetric matrix.

Proof. The following Lyapunov function is considered.

$$V_i(t) = e_i^T(t)Pe_i(t) \quad (25)$$

then

$$\begin{aligned}\dot{V}_i(t) &= \dot{e}_i^T(t)Pe_i(t) + e_i^T(t)P\dot{e}_i(t) \\ &= e_i^T(t) \left(\hat{A}^T P + P\hat{A} + \hat{C}^T \hat{L}^T P + P\hat{L}\hat{C} + \hat{A}^T \hat{C}^T \hat{R}^T P + P\hat{R}\hat{C}\hat{A} \right) e_i(t) \\ &\quad + 2e_i^T(t) [P\hat{I} \quad P(\hat{R}\hat{C}\hat{D} + \hat{D})] \omega_i(t)\end{aligned}\quad (26)$$

The performance index is defined as follows:

$$\begin{aligned} J_i(t) &= \dot{V}_i(t) + \frac{1}{\gamma} e_i^T(t) e_i(t) - \gamma \omega_i^T(t) \omega_i(t) \\ &= \begin{bmatrix} e_i^T(t) & \omega_i^T(t) \end{bmatrix} \Pi \begin{bmatrix} e_i(t) \\ \omega_i(t) \end{bmatrix} \end{aligned} \quad (27)$$

where γ is a scalar, and Π can be defined as follows:

$$\Pi = \begin{bmatrix} P\hat{A} + \hat{A}^T P + P\hat{L}\hat{C} + \hat{C}^T \hat{L}^T P + P\hat{R}\hat{C}\hat{A} + \hat{A}^T \hat{C}^T \hat{R}^T P + \frac{1}{\gamma} I_{12+r} & P\hat{I} & P\hat{L}\hat{C}\hat{D} + P\hat{D} \\ * & -\gamma I_{2r} & 0 \\ * & * & -\gamma I_d \end{bmatrix} \quad (28)$$

For any nonzero $\omega_i(t) \in \mathcal{L}_2[0, \infty)$, $\dot{V}_i(t) + \frac{1}{\gamma} e_i^T(t) e_i(t) - \gamma \omega_i^T(t) \omega_i(t) < 0$ if $\Pi < 0$.

Under the conditions $e_i(0) = 0$, $\int_0^t J_i(\tau) d\tau \leq 0$ and $V_i(t) \geq 0$, the following equation can be proven.

$$\begin{aligned} \int_0^t J_i(\tau) d\tau &= \int_0^t \dot{V}_i(\tau) d\tau + \frac{1}{\gamma} \int_0^t e_i^T(\tau) e_i(\tau) d\tau - \gamma \int_0^t \omega_i^T(\tau) \omega_i(\tau) d\tau \\ &= V_i(t) + \frac{1}{\gamma} \int_0^t e_i^T(\tau) e_i(\tau) d\tau - \gamma \int_0^t \omega_i^T(\tau) \omega_i(\tau) d\tau \\ &\geq \frac{1}{\gamma} \int_0^t e_i^T(\tau) e_i(\tau) d\tau - \gamma \int_0^t \omega_i^T(\tau) \omega_i(\tau) d\tau \end{aligned} \quad (29)$$

Let $t \rightarrow \infty$ in (29), it follows that

$$\int_0^\infty e_i^T(\tau) e_i(\tau) d\tau \leq \gamma^2 \int_0^\infty \omega_i^T(\tau) \omega_i(\tau) d\tau \quad (30)$$

Therefore, the observer error $e_i(t)$ satisfies

$$\|e_i(t)\|_2 \leq \gamma \|\omega_i(t)\|_2 \quad (31)$$

ensuring that the H_∞ norm of the fault observer is less than γ .

Define $Q_1 = P\hat{C}$, $Q_2 = P\hat{R}$ with $Q_1, Q_2 \in \mathbb{R}^{(12+r) \times p}$ and applying the Shur Complement Lemma 3 to Π (28) implies that $\Omega < 0$ if and only if $\Pi < 0$.

$$\Omega = \begin{bmatrix} P\hat{A} + \hat{A}^T P + Q_1\hat{C} + \hat{C}^T Q_1 + Q_2\hat{C}\hat{A} + \hat{A}^T \hat{C}^T Q_2 & P\hat{I} & Q_2\hat{C}\hat{D} + P\hat{D} & I_{12+r} \\ * & -\gamma I_{2r} & 0 & 0 \\ * & * & -\gamma I_d & 0 \\ * & * & * & -\gamma I_{12+r} \end{bmatrix} \quad (32)$$

According to Lemma 2, if Equation (24) holds, the fault estimation error in system (22) exhibits exponential convergence with an α stability margin. \square

3.3. Active Fault-Tolerant Cooperative Controller

In this subsection, an AFTCC law is designed to simultaneously compensate for time-varying faults and ensure formation stability of the leader-following multi-QUAV system. According to Assumption 2, only the relative measurements are permitted for communication among QUAVs. Therefore, the coordinates $(\bar{x}_{d,i}, \bar{y}_{d,i}, \bar{z}_{d,i})$ are defined as the desired relative location between the i -th follower QUAV and the leader.

The leader-following formation achieves stability if

$$\lim_{t \rightarrow \infty} \|\xi_i(t) - \xi_0(t)\| = \bar{\xi}_{d,i} \quad i = 1, 2, \dots, N \quad (33)$$

where $\bar{\xi}_{d,i} = [\bar{x}_{d,i}, 0, \bar{y}_{d,i}, 0, \bar{z}_{d,i}, 0, 0, 0, 0, 0]^T$ is the desired relative position of the i -th QUAV from the leader.

For the i -th QUAV, the relative measurements $\varepsilon_i(t)$ can be written as

$$\varepsilon_i(t) = \sum_{j=1}^N \tilde{a}_{ij} C((\bar{\xi}_{d,i} - \bar{\xi}_{d,j}) - (\xi_i(t) - \xi_j(t))) + w_i C(\bar{\xi}_{d,i} - (\xi_i(t) - \xi_0(t))) \quad (34)$$

where $\tilde{a}_{i,j}$ is the element of the adjacency matrix \tilde{A} and $\tilde{L} = \tilde{D} - \tilde{A}$ with \tilde{D} being the degree matrix; $W = \text{diag}(w_1, w_2, \dots, w_N)$, where $w_i = 1$ if the i -th follower QUAV and the leader are directly connected; $w_i = 0$, otherwise.

Based on Assumption 3, there exists a pseudo-inverse matrix $B^+ \in \mathbb{R}^{m \times 12}$ such that $(I_{12} - BB^+)E = 0$ and the controller can be developed as follows:

$$\begin{cases} u_i(t) = h_i(t)K\varepsilon_i(t) - \hat{f}_{u,i}(t) \\ h_i(t) = \tau_i \varepsilon_i^T(t) \Gamma \varepsilon_i(t) \end{cases} \quad (35)$$

where $h_i(t)$ denotes the time-varying coupling weight of the i -th QUAV, and τ_i is a positive constant. $K \in \mathbb{R}^{m \times 12}$ and $\Gamma \in \mathbb{R}^{p \times p}$ are gain matrices, and $\hat{f}_{u,i}(t)$ represents the deviation between the fault $\hat{f}_i(t)$ estimation and the leader's input estimation $\hat{u}_0(t)$.

According to the input Equation (35), the decoupled dynamic model (18) of the i -th QUAV can be defined as follows:

$$\begin{aligned} \ddot{\xi}_i(t) &= A\bar{\xi}_i(t) + h_i(t)BK\varepsilon_i(t) - B(B^+E\hat{f}_i(t) - \bar{u}_0(t)) - Bu_0(t) + D\bar{d}_i(t) + E\bar{f}_i(t) \\ &= A\bar{\xi}_i(t) + h_i(t)BKC\left(\sum_{j=1}^N \tilde{a}_{ij}((\bar{\xi}_{d,i} - \bar{\xi}_{d,j}) - (\bar{\xi}_i(t) - \bar{\xi}_j(t))) + w_i(\bar{\xi}_{d,i} - \bar{\xi}_i(t))\right) \\ &\quad - B\zeta_{u,i}(t) + D\bar{d}_i(t) + E\zeta_{f,i}(t) \end{aligned} \quad (36)$$

where $\zeta_{u,i} = u_0(t) - \bar{u}_0(t)$ and $\zeta_{f,i} = f_i(t) - \hat{f}_i(t)$.

Similar to the construction of system (8), we define $e_{\xi,i} = \bar{\xi}_{d,i}(t) - \bar{\xi}_i(t)$ and derive the overall error dynamics (36) as follows:

$$\begin{cases} \dot{e}_{\xi}(t) = (I_N \otimes A - H\tilde{L} \otimes BKC)e_{\xi}(t) + (I_N \otimes B)\zeta_u(t) \\ \quad - (I_N \otimes D)\bar{d}(t) - (I_N \otimes E)\zeta_f \\ \quad - (I_N \otimes A)\bar{\xi}_d(t), \\ \dot{h}_i(t) = \tau_i [\tilde{l}_{ij} C e_{\xi,j}(t)]^T \Gamma [\tilde{l}_{ij} C e_{\xi,j}(t)] \end{cases} \quad (37)$$

where \tilde{l}_{ij} is the element of the Laplacian matrix $\tilde{L} \in \mathbb{R}^{N \times N}$ and $H = \text{diag}(h_1, h_2, \dots, h_N)$; $e_{\xi}(t) = [e_{\xi,1}^T(t), e_{\xi,2}^T(t), \dots, e_{\xi,N}^T(t)]^T$. $\zeta_f(t)$ and $\zeta_u(t)$ denote $[\zeta_{f,1}(t), \zeta_{f,2}(t), \dots, \zeta_{f,N}(t)]^T$ and $[\zeta_{u,1}(t), \zeta_{u,2}(t), \dots, \zeta_{u,N}(t)]^T$, respectively.

Define $T = [I_N \otimes B, -I_N \otimes D, -I_N \otimes E, -I_N \otimes A]$ and $\eta(t) = [\zeta_u^T(t), \bar{d}^T(t), \zeta_f^T(t), \bar{\xi}_d^T(t)]^T$, where $\zeta_u^T(t), \bar{d}^T(t), \zeta_f^T(t)$ and $\bar{\xi}_d^T(t)$ are bounded.

$$\begin{cases} \dot{e}_{\xi}(t) = (I_N \otimes A - H\tilde{L} \otimes BKC)e_{\xi}(t) + T\eta(t) \\ \dot{h}_i(t) = \tau_i [\tilde{l}_{ij} C e_{\xi,j}(t)]^T \Gamma [\tilde{l}_{ij} C e_{\xi,j}(t)] \end{cases} \quad (38)$$

Theorem 2. For given scales $\gamma > 0$ and $\beta > 0$, the error dynamic (38) is asymptotically stable and the H_∞ norm of the error system is less than γ if there exists a positive definite symmetric matrix X such that the following LMI holds:

$$\Xi_i = \begin{bmatrix} \Xi_{i,11} & \lambda_i XB & -\lambda_i XD & -\lambda_i XE & -\lambda_i XA & I_{12} \\ * & -\gamma I_m & 0 & 0 & 0 & 0 \\ * & * & -\gamma I_d & 0 & 0 & 0 \\ * & * & * & -\gamma I_r & 0 & 0 \\ * & * & * & * & -\gamma I_{12} & 0 \\ * & * & * & * & * & -\gamma I_{12} \end{bmatrix} \quad (39)$$

where $\Xi_{i,11} = \lambda_i(XA + A^T X) - 2\beta\lambda_i^2 QC$, $Q = C^T \Gamma = XBK$ with $Q \in \mathbb{R}^{12 \times 12}$ and λ_i for $i = 1, 2, \dots, N$ are the eigenvalues of \tilde{L} . * denotes the symmetric item in this matrix.

Proof. Considering the following Lyapunov function:

$$V(t) = e_\xi^T(t)(\tilde{L} \otimes X)e_\xi(t) + \sum_{j=1}^N \frac{(h_i(t) - \beta)^2}{\tau_i} \quad (40)$$

The derivative of $V(t)$ in (40) is derived as follows:

$$\begin{aligned} \dot{V}(t) &= e_\xi^T(t) \left[\tilde{L} \otimes (XA + A^T X) \right] e_\xi(t) + 2e_\xi^T(t)(\tilde{L} \otimes X)T\eta(t) \\ &\quad - 2e_\xi^T(t)(\tilde{L}H\tilde{L} \otimes XBKC)e_\xi(t) + 2 \sum_{i=1}^N h_i(t) \left(\sum_{j=1}^N \tilde{l}_{ij} C^T e_{\xi,j}^T(t) \right) \Gamma \left(\sum_{j=1}^N \tilde{l}_{ij} C e_{\xi,j}(t) \right) \\ &\quad - 2\beta \sum_{i=1}^N \left(\sum_{j=1}^N \tilde{l}_{ij} C^T e_{\xi,j}^T(t) \right) \Gamma \left(\sum_{j=1}^N \tilde{l}_{ij} C e_{\xi,j}(t) \right) \end{aligned} \quad (41)$$

To simplify the expression by reducing the quadratic terms in Equation (41), we introduce the constraint $C^T \Gamma = XBK = Q$. The quadratic form of the double summation can be expressed as follows:

$$2 \sum_{i=1}^N h_i(t) \left(\sum_{j=1}^N \tilde{l}_{ij} C^T e_{\xi,j}^T(t) \right) \Gamma \left(\sum_{j=1}^N \tilde{l}_{ij} C e_{\xi,j}(t) \right) = 2e_\xi^T(t)(\tilde{L}H\tilde{L} \otimes C^T \Gamma C)e_\xi(t) \quad (42)$$

Then, the $\dot{V}(t)$ can be simplified as follows:

$$\begin{aligned} \dot{V}(t) &= e_\xi^T(t) \left[\tilde{L} \otimes (XA + A^T X) \right] e_\xi(t) + 2e_\xi^T(t)(\tilde{L} \otimes X)T\eta(t) \\ &\quad - 2\beta e_\xi^T(t)(\tilde{L}^2 \otimes C^T \Gamma C)e_\xi(t) \\ &= e_\xi^T(t) \left[\tilde{L} \otimes (XA + A^T X) - 2\beta \tilde{L}^2 \otimes QC \right] e_\xi(t) + 2e_\xi^T(t)(\tilde{L} \otimes X)T\eta(t) \end{aligned} \quad (43)$$

Similar to the proof from (26) to (32), the error dynamics (39) are asymptotically stable with H_∞ performance less than γ if the following holds.

$$\begin{bmatrix} \tilde{L} \otimes (XA + A^T X) - 2\beta \tilde{L}^2 \otimes QC & \tilde{L} \otimes XB & -\tilde{L} \otimes XD & -\tilde{L} \otimes XE & \tilde{L} \otimes XA & I_N \otimes I_{12} \\ * & -\gamma I_N \otimes I_m & 0 & 0 & 0 & 0 \\ * & * & -\gamma I_N \otimes I_d & 0 & 0 & 0 \\ * & * & * & -\gamma I_N \otimes I_r & 0 & 0 \\ * & * & * & * & -\gamma I_N \otimes I_{12} & 0 \\ * & * & * & * & * & -\gamma I_N \otimes I_{12} \end{bmatrix} < 0 \quad (44)$$

Based on Lemma 1, there exists symmetric matrix V such that

$$\Theta = V^T \tilde{L} V \quad (45)$$

where $\Theta = \text{diag}(\lambda_1, \lambda_2, \dots, \lambda_N)$.

Define $\tilde{V} = \text{diag}(V_T \otimes I_{12}, V_T \otimes I_m, V_T \otimes I_d, V_T \otimes I_r, V_T \otimes I_{12}, V_T \otimes I_{12})$, let matrix in (44) left multiplying \tilde{V} and right multiplying \tilde{V}^T , and we can derive

$$\begin{bmatrix} \Theta \otimes (XA + A^T X) - 2\beta \Theta \tilde{L} \otimes QC & \Theta \otimes XB & -\Theta \otimes XD & -\Theta \otimes XE & \Theta \otimes XA & I_N \otimes I_{12} \\ * & -\gamma I_N \otimes I_m & 0 & 0 & 0 & 0 \\ * & * & -\gamma I_N \otimes I_d & 0 & 0 & 0 \\ * & * & * & -\gamma I_N \otimes I_r & 0 & 0 \\ * & * & * & * & -\gamma I_N \otimes I_{12} & 0 \\ * & * & * & * & * & -\gamma I_N \otimes I_{12} \end{bmatrix} < 0 \quad (46)$$

Applying appropriate matrix transformation, the matrix (46) can be transformed into

$$\Xi = \begin{bmatrix} \Xi_1 & 0 & \cdots & 0 \\ 0 & \Xi_2 & \cdots & 0 \\ \vdots & \vdots & \ddots & \vdots \\ 0 & 0 & \cdots & \Xi_N \end{bmatrix} < 0 \quad (47)$$

$\Xi < 0$ if and only if $\Xi_i < 0$, for $i = 1, 2, \dots, N$. \square

4. Simulation

In this section, the effectiveness of the fault estimation observer (19) and AFTCC law (35) is demonstrated through simulation studies. The simulation is organized into four parts: experimental setup, fault-tolerant control performance, performance analysis, and comparative study.

4.1. Experimental Conditions

A leader-following multi-QUAV system with one leader and three followers is considered, where each QUAV is equipped with relative measurement devices. The system parameters are set as follows: $L = 0.2$ m, $K_y = 4$ m, $m = 1.42$ kg, $g = 9.81$ m/s², $I_x = 0.03$ kg · m², $I_y = 0.03$ kg · m², and $I_z = 0.04$ kg · m². The matrices are configured as $D = 0.1 * \mathbf{1}_{12}$ and $E = B$, considering bounded actuator faults in the four brushless motors. The output matrix $C = I_{12}$. External disturbances are simulated using sinusoidal signals.

Each follower QUAV can interact with neighboring follower QUAVs; however, only one follower QUAV is granted a unidirectional communication link to the leader as shown in Figure 2. Therefore, the communication topology among the four QUAVs can be described as follows:

$$\mathcal{L} = \begin{bmatrix} 0 & 0 & 0 & 0 \\ -1 & 3 & -1 & -1 \\ 0 & -1 & 2 & -1 \\ 0 & -1 & -1 & 2 \end{bmatrix} \quad (48)$$

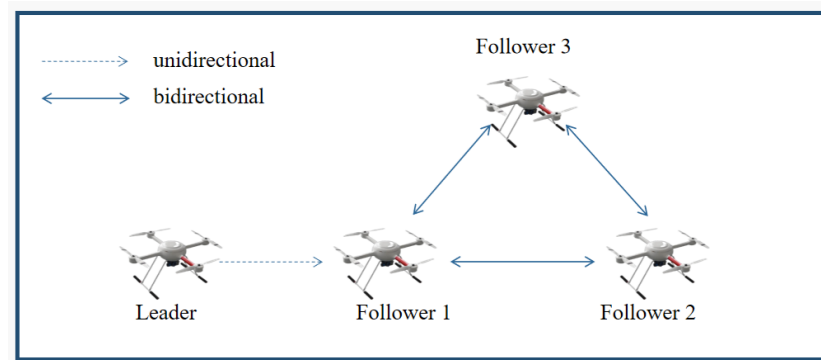


Figure 2. Communication network topology.

Assuming that QUAVs are operating in extreme flight conditions, where each follower QUAV is subjected to time-varying actuator faults at distinct time instants, the actuator faults are modeled as follows. A step signal fault occurs in the 3rd motor of follower QUAV 1 at $t = 50$ s.

$$f_{1,3}(t) = \begin{cases} 0 & t < 50 \text{ s} \\ 5 & t \geq 50 \text{ s} \end{cases} \quad (49)$$

Subsequently, a step signal fault is introduced into the 2nd motor of follower QUAV 2 at $t = 100$ s.

$$f_{2,2}(t) = \begin{cases} 0 & t < 100 \text{ s} \\ 8 & t \geq 100 \text{ s} \end{cases} \quad (50)$$

Later in the following QUAV 3, the fault situation of the 1st and 4th motor is

$$f_{3,1}(t) = \begin{cases} 0 & t < 150 \text{ s} \\ 20 \sin(0.1t) & t \geq 150 \text{ s} \end{cases}, \quad f_{3,4}(t) = \begin{cases} 0 & t < 150 \text{ s} \\ 20 \sin(0.1t) & t \geq 150 \text{ s} \end{cases} \quad (51)$$

After applying transformation and scaling, the decoupled system in the form of (18) can be derived, and the fault estimation observer analogous to (19) for each decoupled system can be obtained. The observer gain matrix and controller gain matrix can be obtained via LMI optimization.

For the fault estimation observer, the gain matrices are

$$G = \begin{bmatrix} 0.0475 & -6.8729 & 0.0475 & -6.8719 & 0.0475 & -7.0242 & 1.3987 & -6.8675 & -1.3887 & -6.9494 & 0.0475 & -6.8789 \\ 0.0249 & -4.4976 & 0.0250 & -4.4972 & 0.0250 & -4.6639 & 0.9079 & -4.4956 & -0.9136 & -4.4273 & 0.0249 & -4.5016 \\ 0.0467 & -6.7937 & 0.0467 & -6.7927 & 0.0467 & -6.9458 & 1.3819 & -6.8632 & -1.3729 & -6.7971 & 0.0468 & -6.7901 \\ 0.0242 & -4.4185 & 0.0242 & -4.4181 & 0.0242 & -4.5856 & 0.8915 & -4.3415 & -0.8983 & -4.4199 & 0.0242 & -4.4127 \end{bmatrix} \quad (52)$$

$$R = \begin{bmatrix} 6.9406 & 0.1905 & 6.9416 & 0.0922 & 6.7891 & -34.2872 & 6.9456 & 0.0280 & 6.8663 & -7.2000 & 6.9369 & -0.2435 \\ 4.5188 & 0.0535 & 4.5192 & 0.1104 & 4.3524 & -34.2660 & 4.5208 & 0.0436 & 4.5937 & 7.2750 & 4.5174 & -0.2387 \\ 6.8692 & 0.1945 & 6.8702 & 0.1070 & 6.7170 & -34.2373 & 6.8005 & -7.2735 & 6.8661 & -0.0274 & 6.8748 & 0.2390 \\ 4.4560 & 0.0618 & 4.4564 & 0.1293 & 4.2891 & -34.2396 & 4.5298 & 7.2015 & 4.4551 & -0.0431 & 4.4599 & 0.2438 \end{bmatrix} \quad (53)$$

$$S = 10^3 \times \begin{bmatrix} 0.6643 & -0.3228 & 0.6643 & -0.3288 & 0.6383 & -1.9679 & 0.0744 & -0.3332 & -0.0610 & -0.6786 & 0.6638 & -0.3442 \\ 0.4325 & -0.2134 & 0.4325 & -0.2116 & 0.4051 & -1.8511 & 0.0483 & -0.2157 & -0.0394 & 0.1292 & 0.4322 & -0.2278 \\ 0.6574 & -0.3189 & 0.6575 & -0.3244 & 0.6314 & -1.9618 & 0.0734 & -0.6778 & -0.0602 & -0.3325 & 0.6580 & -0.3174 \\ 0.4264 & -0.2103 & 0.4265 & -0.2079 & 0.3991 & -1.8471 & 0.0479 & 0.1286 & -0.0391 & -0.2173 & 0.4269 & -0.2020 \end{bmatrix} \quad (54)$$

For the AFTCC law, the parameters are $\beta = 3$, $\tau_i = 0.01$, for $i = 1, 2, \dots, N$.

$$K = \begin{bmatrix} 0.0099 & 0.0858 & 0.0005 & -0.0007 & 0.1843 & 0.4224 & 0.0008 & -0.0004 & 0.0964 & 0.5788 & 0.0432 & 0.2789 \\ -0.0086 & -0.0845 & 0.0009 & -0.0006 & 0.1858 & 0.4222 & 0.0013 & -0.0001 & -0.0952 & -0.5795 & 0.0431 & 0.2781 \\ 0.0007 & 0.0005 & -0.0061 & -0.0879 & 0.1852 & 0.4221 & 0.1201 & 0.5782 & 0.0007 & 0.0001 & -0.0417 & -0.2789 \\ 0.0014 & 0.0012 & 0.0078 & 0.0869 & 0.1851 & 0.4227 & -0.1181 & -0.5779 & 0.0007 & 0.0004 & -0.0408 & -0.2791 \end{bmatrix} \quad (55)$$

$$\Gamma = \begin{bmatrix} 67.7650 & 16.2860 & 0.0243 & -0.0565 & 0.0007 & -0.0002 & 0.0431 & -0.0467 & 0.9261 & -1.5739 & 0.0005 & -0.0049 \\ 12.1037 & 70.6070 & -0.0852 & -0.0278 & -0.0430 & -0.0334 & -0.0123 & -0.0234 & 2.3345 & -2.9932 & -0.0418 & -0.0172 \\ -0.0286 & 0.0090 & 67.7543 & 16.6981 & -0.0023 & -0.0257 & 0.1377 & 1.1740 & -0.0041 & -0.0621 & 0.0065 & -0.0614 \\ -0.0311 & -0.0189 & 11.6521 & 70.6005 & -0.0282 & -0.0124 & -3.8572 & 3.2429 & -0.0349 & -0.0138 & -0.0604 & -0.0183 \\ 0.0077 & -0.0209 & 0.0020 & -0.0621 & 69.0785 & 8.6184 & 0.0361 & -0.0937 & -0.0077 & 0.0242 & -0.0090 & -0.0574 \\ -0.0401 & -0.0290 & -0.0294 & -0.0798 & 9.9525 & 64.7698 & 0.0092 & -0.0476 & -0.0282 & -0.0793 & -0.0051 & -0.0636 \\ -0.0019 & -0.0410 & -0.9990 & -0.4592 & 0.0095 & -0.0198 & 53.7888 & 3.6454 & -0.0148 & -0.0208 & 0.0163 & -0.0665 \\ -0.0470 & -0.0311 & 1.2286 & -0.2129 & -0.0065 & -0.0447 & 12.0085 & 69.6938 & -0.0058 & -0.0259 & -0.0731 & 0.0057 \\ -0.0113 & 1.8854 & 0.0069 & -0.0301 & 0.0217 & 0.0025 & 0.0448 & -0.0592 & 53.7644 & 6.2425 & 0.0084 & -0.0399 \\ -1.0122 & -0.1265 & -0.0257 & -0.0286 & -0.0982 & 0.0098 & -0.0374 & -0.0162 & 9.4300 & 69.7090 & 0.0044 & 0.0493 \\ 0.0017 & -0.0285 & -0.0146 & -0.0382 & 0.0149 & -0.0423 & 0.0275 & -0.0304 & -0.0020 & -0.0866 & 67.4874 & 15.7348 \\ -0.0695 & -0.0329 & -0.0267 & -0.0212 & -0.0200 & -0.0120 & 0.0084 & -0.0607 & -0.0140 & -0.0875 & 13.6255 & 90.0328 \end{bmatrix} \quad (56)$$

4.2. Fault-Tolerant Control Performance

This subsection demonstrates the effectiveness of the proposed AFTCC method through simulation of a formation transition task. The multi-QUAV system adopts a linear formation configuration with adjacent QUAVs separated by 5 m. The leader QUAV is controlled by a PID controller and maintains a constant velocity $V_x = 2$ m/s along the x-axis. The solver used in the simulation is odes15.

The trajectory of the multi-QUAVs in the inertial frame is shown in Figure 3.

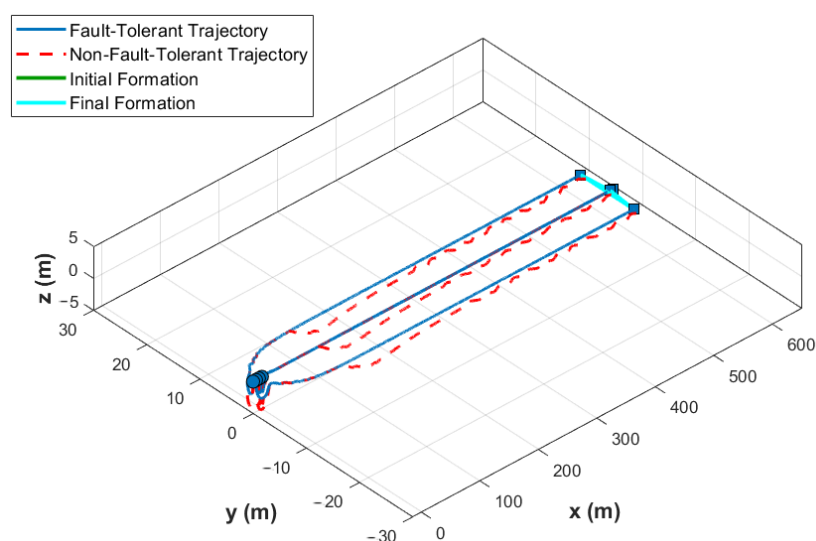


Figure 3. The trajectory of the multi-QUAVs.

The simulation results are presented in the following figures.

Figure 4 illustrates the relative position of the follower QUAVs under multiple faults conditions, without the active fault-tolerant control law (35) proposed by this paper. It is evident that a single fault in one of the follower QUAVs causes the collapse of the consensus-based formation.

Figures 5–7 show fault estimation results of follower QUAVs based on the fault estimation observer (19). As shown in Figures 5–7, the fault estimation observer can accurately estimate the time-varying actuator faults and the inputs of the leader QUAV.

Then, the estimation of actuator faults and inputs of the leader is used in the active fault-tolerant control law (39), and the consensus-based formation results of multi-QUAVs is shown as follows.

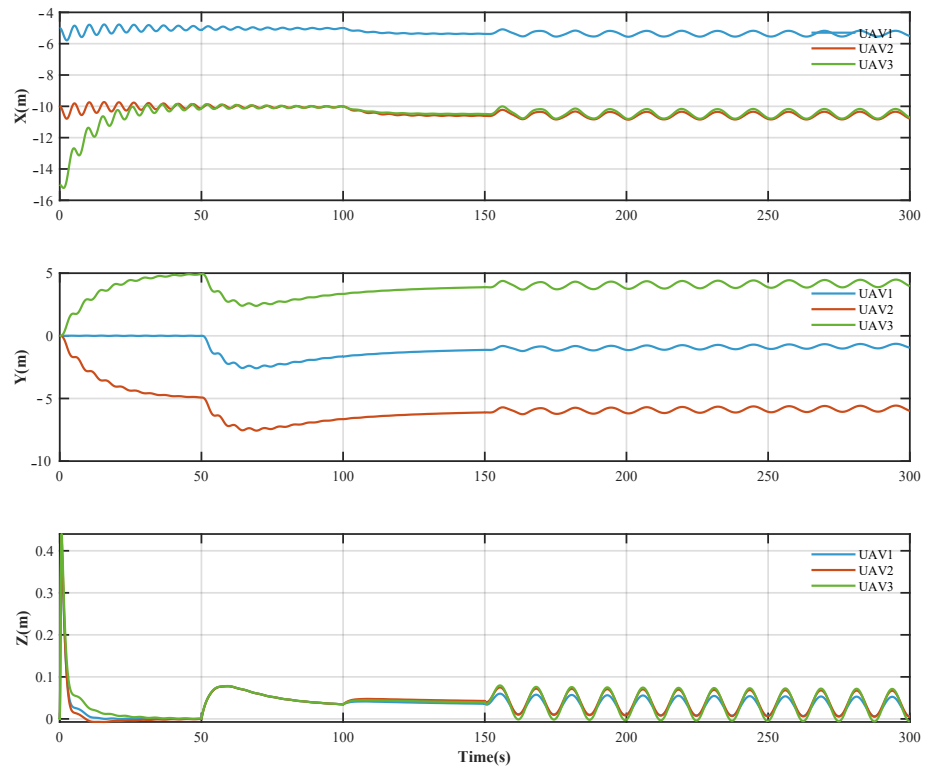


Figure 4. Relative position of QUAVs under non-fault-tolerant control.

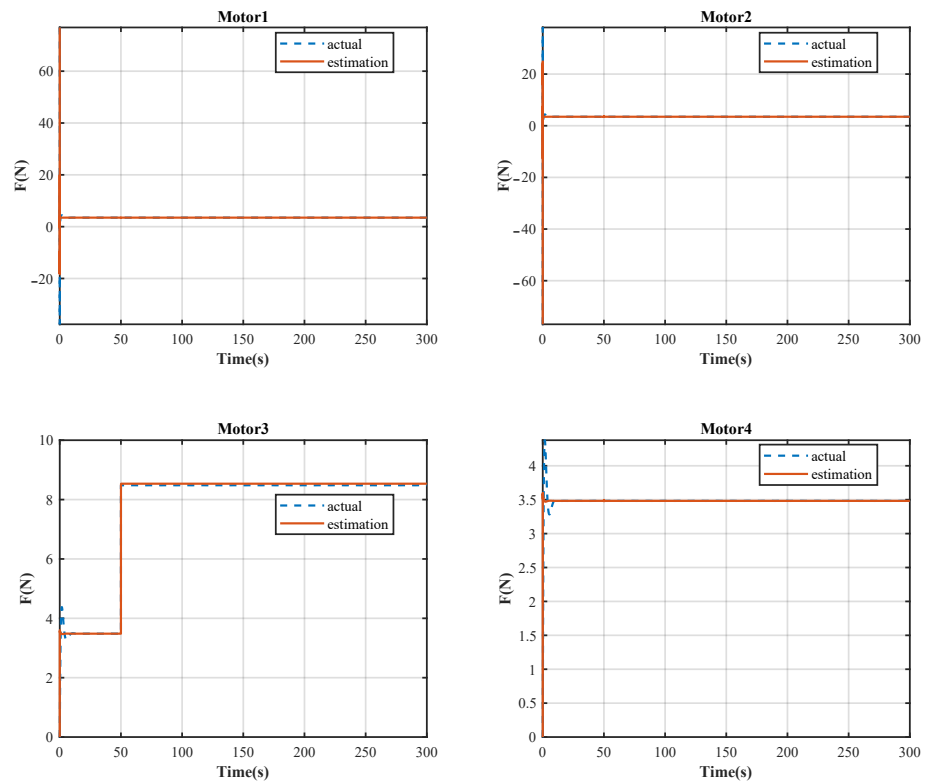


Figure 5. The fault reconstruction of QUAV 1.

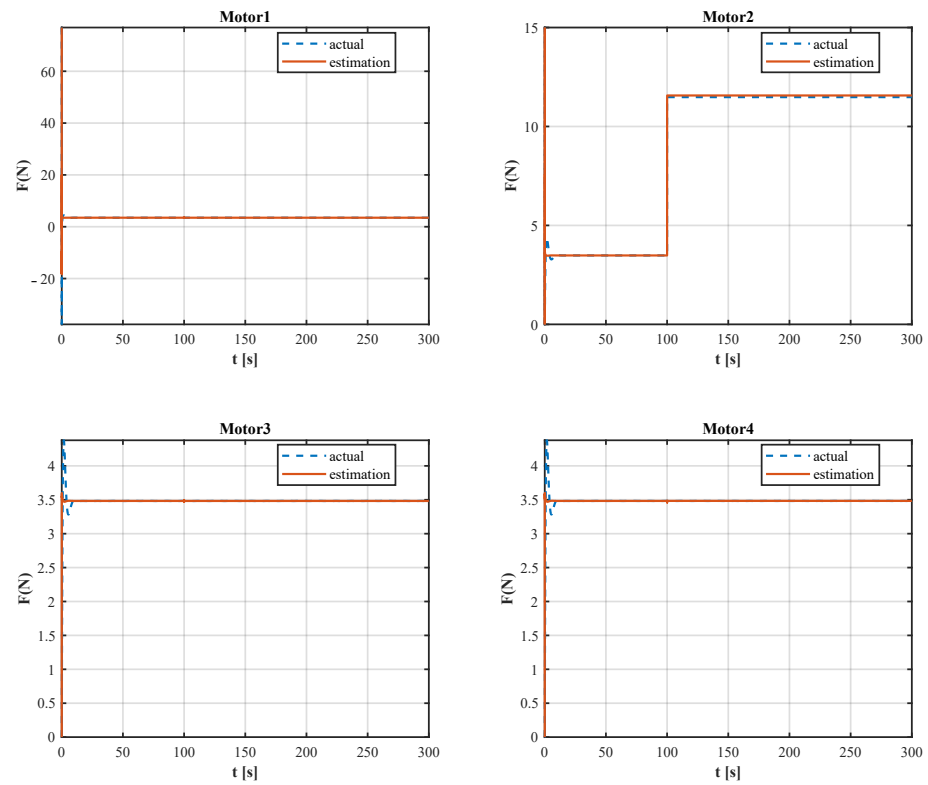


Figure 6. The fault reconstruction of QUAV 2.

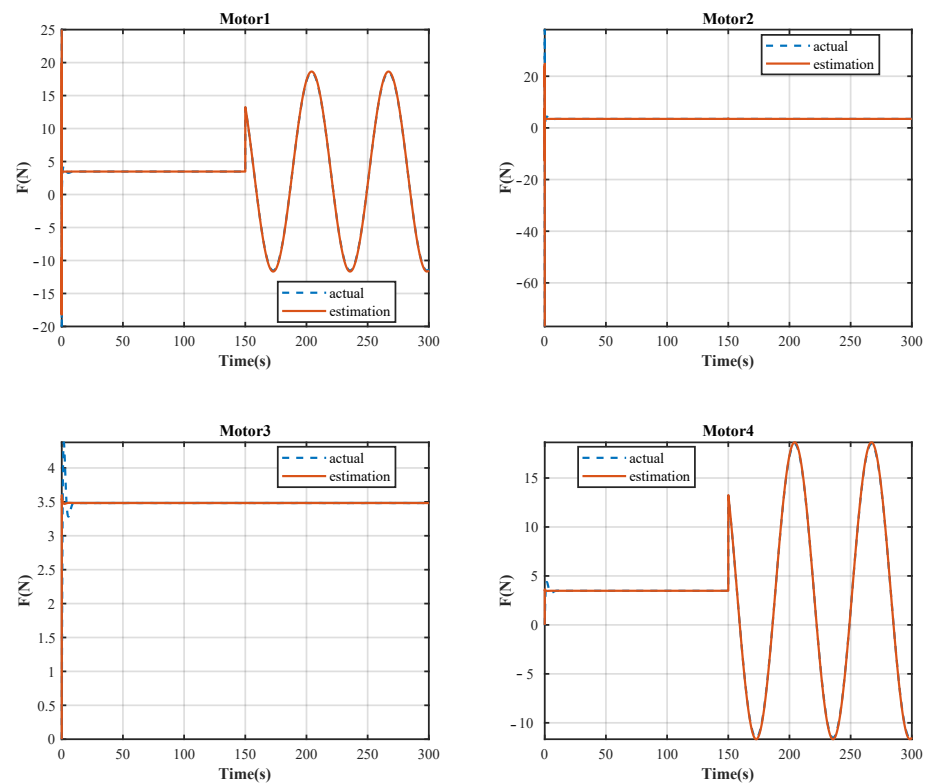


Figure 7. The fault reconstruction of QUAV 3.

From Figure 8, it is evident that the control law (39) can accurately keep a consensus-based formation by quickly reconstructing the fault signals via the fault estimation observer. Comparing Figure 4 to Figure 8 demonstrates the effectiveness of the AFTCC scheme proposed by this paper.

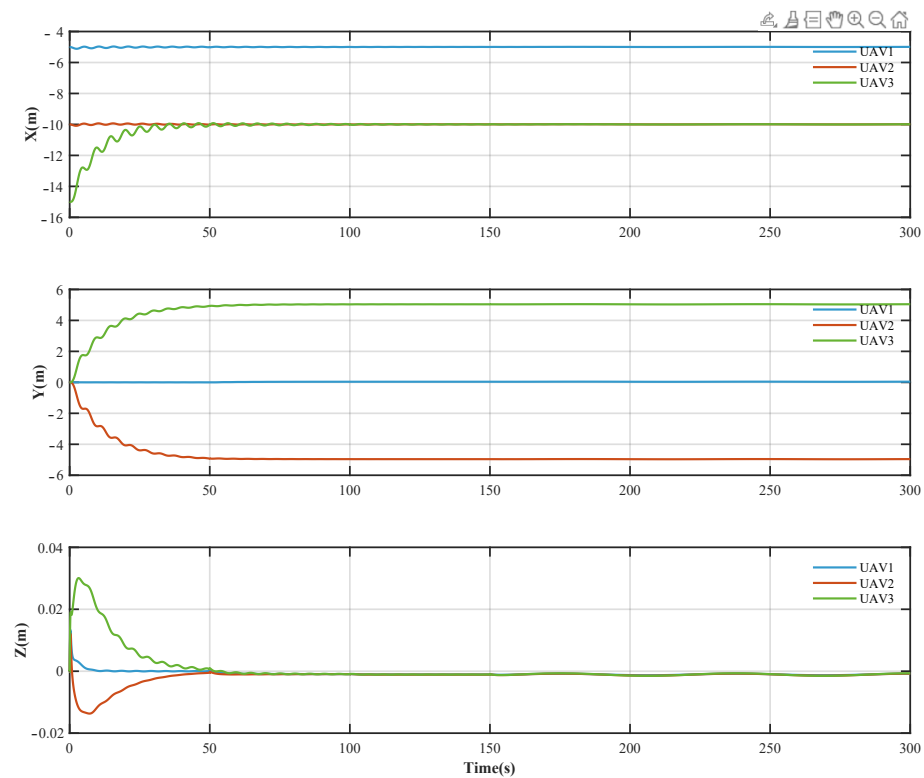


Figure 8. Relative position of QUAUVs under fault-tolerant control.

4.3. Performance Analysis

To further quantify the formation tracking performance and numerically validate the effectiveness of the proposed AFTCC, the root-mean-square error (RMSE) is calculated for position tracking accuracy assessment. The position-tracking error of the i -th follower QUAUV is defined as

$$e_{p,i}(t) = C_p e_{\zeta,i}(t) \quad (57)$$

where C_p is as follows:

$$C_p = \begin{bmatrix} 1 & 0 & 0 & 0 & 0 & 0 & 0 & 0 & 0 & 0 & 0 & 0 \\ 0 & 0 & 1 & 0 & 0 & 0 & 0 & 0 & 0 & 0 & 0 & 0 \\ 0 & 0 & 0 & 0 & 1 & 0 & 0 & 0 & 0 & 0 & 0 & 0 \end{bmatrix}$$

The position RMSE is calculated as follows:

$$\text{RMSE}_{p,i} = \sqrt{\frac{1}{M} \sum_{k=1}^M \|e_{p,i}[k]\|_2^2}. \quad (58)$$

The calculated results are summarized in Table 1.

Table 1. Position tracking RMSE for follower QUAUVs under the proposed AFTCC (in meters).

Follower	Time Interval (s)	RMSE _p (m)
QUAV 1	[50, 300]	0.0366
QUAV 2	[100, 300]	0.0408
QUAV 3	[150, 300]	0.0411

As shown in Table 1, the position RMSE values remain consistently small, with all followers maintaining tracking errors below 0.05 m. These results confirm the effectiveness of the proposed AFTCC in maintaining precise formation tracking under actuator faults.

4.4. Comparative Experiment

To further validate the effectiveness of the proposed method, a comparative study is conducted with an existing relative-information-based fault-tolerant control approach from the literature [36]. Both methods are tested under identical conditions using the same multi-QUAV system configuration and fault scenarios.

The comparison is performed with the same actuator fault conditions as described previously, where faults occur at $t = 50$ s, $t = 100$ s, and $t = 150$ s for follower QUAVs 1, 2, and 3, respectively. Figure 9 illustrates the comparative position tracking performance of both methods.

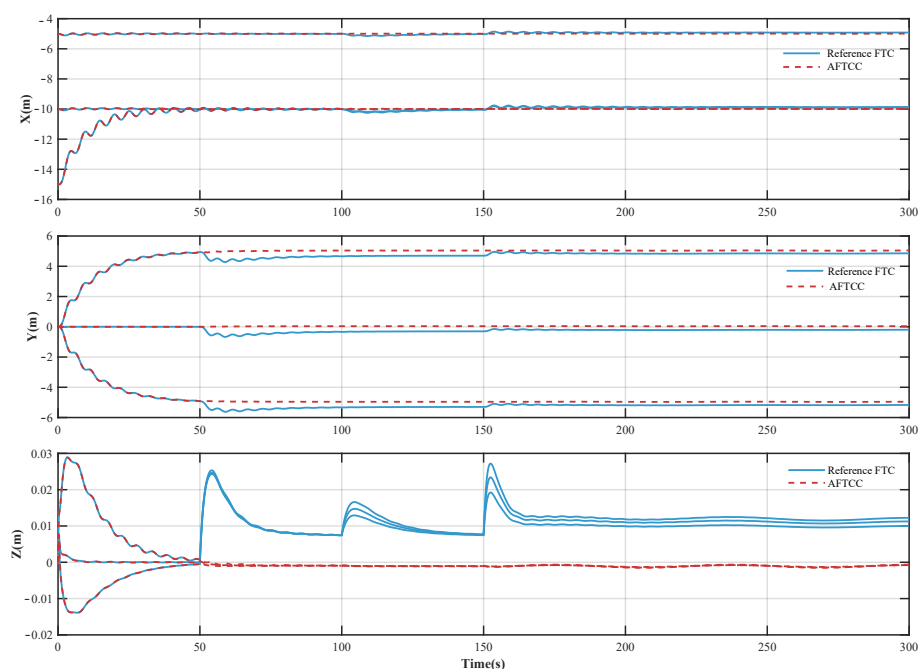


Figure 9. Position tracking comparison between the proposed AFTCC and reference method.

From Figure 9, it can be observed that both the proposed AFTCC and the reference method can maintain formation stability under actuator faults. However, the proposed method demonstrates superior performance characteristics. Specifically, the proposed AFTCC achieves faster fault response and more accurate position tracking with reduced transient oscillations compared to the reference approach. This improvement can be attributed to the proportional-integral mechanism incorporated in the fault estimation observer, which enables faster and more accurate tracking performance.

5. Conclusions

In this paper, appropriate translation and scaling are applied to multi-QUAVs with relative measurements, and a decoupled observable system is obtained. After deriving the decoupled dynamics, an adaptive fault estimation observer is designed and proves that it is asymptotically stable with H_∞ performance. Subsequently, a consensus-based AFTCC law is proposed to quickly compensate for the time-varying actuator faults. Finally, the effectiveness of the proposed AFTCC is verified by simulations under multiple fault conditions. The RMSE analysis shows that the proposed method maintains precise formation

tracking performance. Comparative results demonstrate the superior performance of the proposed approach over existing methods.

Author Contributions: Conceptualization, Y.Z. and X.C.; methodology, Y.Z.; software, P.L.; validation, P.L., X.C., and P.H.; formal analysis, Y.Z. and X.C.; investigation, Y.Z.; resources, Y.Z.; data curation, P.L.; writing—original draft preparation, X.C.; writing—review and editing, K.N.; visualization, X.C.; supervision, Y.Z.; project administration, Z.W.; funding acquisition, Z.W. All authors have read and agreed to the published version of the manuscript.

Funding: The authors disclosed receipt of the following financial support for the research, authorship, and/or publication of this article: This work was supported by the Natural Science Foundation of Shaanxi Province (2025JC-YBQN-809).

Institutional Review Board Statement: Not applicable.

Informed Consent Statement: Not applicable.

Data Availability Statement: The data generated during the current study are available from the corresponding author on reasonable request.

Conflicts of Interest: Author Kunlin Nie was employed by the company Acyber. The remaining authors declare that the research was conducted in the absence of any commercial or financial relationships that could be construed as a potential conflict of interest.

References

- Shi, M.; Zhang, X.; Chen, J.; Cheng, H. UAV Cluster-Assisted Task Offloading for Emergent Disaster Scenarios. *Appl. Sci.* **2023**, *13*, 4724. [\[CrossRef\]](#)
- Rashid, A.B.; Kausik, A.K.; Khandoker, A.; Siddique, S.N. Integration of Artificial Intelligence and IoT with UAVs for Precision Agriculture. *Hybrid Adv.* **2025**, *10*, 100458. [\[CrossRef\]](#)
- Adnan, M.H.; Zukarnain, Z.A.; Subramaniam, S.K. Path Planning for Multi-UAV-Assisted Mobile Edge Computing Framework Using Reinforcement Learning in Urban Environment Disaster Scenarios. *Ad Hoc Netw.* **2025**, *178*, 103928. [\[CrossRef\]](#)
- Jond, H.B.; Beaver, L.E.; Jiroušek, M.; Ahmadlou, N.; Bakircioğlu, V.; Saska, M. Flatness-Based Finite-Horizon Multi-UAV Formation Trajectory Planning and Directionally Aware Collision Avoidance Tracking. *J. Franklin Inst.* **2025**, *362*, 107867. [\[CrossRef\]](#)
- Gonzalez, V.; Jaillet, P. Multi-Drone Rescue Search in a Large Network. *Eur. J. Oper. Res.* **2025**, *324*, 787–798. [\[CrossRef\]](#)
- Cao, Z.; Chen, G. Enhanced Deep Reinforcement Learning for Integrated Navigation in Multi-UAV Systems. *Chin. J. Aeronaut.* **2025**, *38*, 103497. [\[CrossRef\]](#)
- Zhang, P.; Li, G. A Cooperative Dynamic Target Search Approach for Multi-UAV Systems Utilizing the MAPPO Algorithm. *Discov. Artif. Intell.* **2025**, *5*, 153. [\[CrossRef\]](#)
- Wang, W.; Chen, Y.; Zhang, Y.; Chen, Y.; Du, Y. Collaborative Search Algorithm for Multi-UAVs Under Interference Conditions: A Multi-Agent Deep Reinforcement Learning Approach. *Drones* **2025**, *9*, 445. [\[CrossRef\]](#)
- Gao, H.; Zhang, A.; Li, W.; Cai, H. Drone Swarm Robust Cooperative Formation Pursuit through Relative Positioning in a Location Denial Environment. *Drones* **2024**, *8*, 455. [\[CrossRef\]](#)
- Guzey, H.M. Adaptive Consensus-Based Formation Control of Fixed-Wing MUAVs. In Proceedings of the 2017 IEEE 4th International Conference on Actual Problems of Unmanned Aerial Vehicles Developments (APUAVD), Kyiv, Ukraine, 17–19 October 2017; IEEE: Piscataway, NJ, USA, 2017; pp. 184–187. [\[CrossRef\]](#)
- Xiang, Y.; Li, S.; Li, R.; Zhao, Z.; Zhang, H. Decentralized Consensus Inference-Based Hierarchical Reinforcement Learning for Multiconstrained UAV Pursuit-Evasion Game. *IEEE Trans. Neural Netw. Learn. Syst.* **2025**, *Early Access*. [\[CrossRef\]](#)
- Liu, P.-M.; Guo, X.-G.; Wang, J.-L.; Lu, H.; Wu, Z.-G. Switching Function-Based Optimal Active Fault-Tolerant Bipartite Consensus Control for UAV Swarm. *Automatica* **2025**, *179*, 112440. [\[CrossRef\]](#)
- Xiao, L.; Xiao, Z.; Fu, Z.; Cheng, C.; Li, F.; Yang, Y. Multiple UAV Cooperative Substation Inspection: A Robust Fixed-Time Group Formation Control Scheme. *Symmetry* **2025**, *17*, 857. [\[CrossRef\]](#)
- Li, J.; Wang, H.; Wang, Y.; Zhang, M.; Ren, B.; Zhu, J. Terminal constraint guidance and predefined-time event-triggered consensus control for multi-UAV aerial rendezvous. *Nonlinear Dyn.* **2025**, *113*, 16695–16720. [\[CrossRef\]](#)
- Li, Y.; Li, A.; Zhang, Z.; Song, G. Fault-Tolerant Control of Nonlinear Cluster System for Fixed-Wing UAV Piston Engine Faults Based on Hierarchical Architecture. *Aerosp. Sci. Technol.* **2025**, *157*, 109804. [\[CrossRef\]](#)

16. Guo, G.; Xiao, S.; Chen, F.; Hou, Z.; Tan, H. Dynamic Event-Triggered Predefined-Time Adaptive Attitude Fault-Tolerant Control for Uncertain Unmanned Aerial Vehicles with Disturbances and Actuator Faults. *Aerosp. Sci. Technol.* **2025**, *165*, 110481. [\[CrossRef\]](#)
17. Hu, J.; Xu, Y.; Jiang, B. Game-Based Fault-Tolerant Formation Containment Control for Fixed-Wing UAVs Under the Fully Actuated System Framework. *Aerosp. Sci. Technol.* **2025**, *160*, 110052. [\[CrossRef\]](#)
18. Cai, J.; Lovera, M. Passive Fault-Tolerant Control of Dual-System UAV Transition Flight Under Partial Loss of Propellers. *Aerotec. Missili Spaz.* **2025**, *102*, 131–143. [\[CrossRef\]](#)
19. Wang, W.; Chen, Y.; Ren, Z.; Liu, H. Two-Step Robust Fault-Tolerant Controller Design Based on Nonlinear Extended State Observer (NESO) for Unmanned Aerial Vehicles (UAVs) with Actuator Faults and Disturbances. *Drones* **2025**, *9*, 183. [\[CrossRef\]](#)
20. Wang, L.; Li, A.; Lu, H.; Wang, C.; Zabolotnov, Y. Distributed Adaptive Event-Triggered Finite-Time Fault-Tolerant Containment Control for Multi-UAVs with Input Constraints and Actuator Failures. *J. Franklin Inst.* **2024**, *361*, 107308. [\[CrossRef\]](#)
21. Liu, C.; Jiang, B.; Patton, R.J.; Zhang, K. Integrated Fault-Tolerant Control for Close Formation Flight. *IEEE Trans. Aerosp. Electron. Syst.* **2019**, *55*, 3257–3267. [\[CrossRef\]](#)
22. Yin, L.; Liu, J.; Yang, P.; Shi, J. Sliding Mode Observer-Based Active Fault-Tolerant Control for UAVs Formation. *IOP Conf. Ser. Mater. Sci. Eng.* **2018**, *452*, 042068. [\[CrossRef\]](#)
23. Yang, Z.; Li, M.; Yu, Z.; Cheng, Y.; Xu, G.; Zhang, Y. Fault Detection and Fault-Tolerant Cooperative Control of Multi-UAVs under Actuator Faults, Sensor Faults, and Wind Disturbances. *Drones* **2023**, *7*, 503. [\[CrossRef\]](#)
24. Zhu, J.W.; Yang, G.H.; Zhang, W.A.; Yu, L. Cooperative Fault-Tolerant Tracking Control for Multiagent Systems: An Intermediate Estimator-Based Approach. *IEEE Trans. Cybern.* **2017**, *47*, 3890–3899. [\[CrossRef\]](#)
25. Luo, F.; Zhou, D.; Li, Y.; Liu, K. An Active and Passive Combined Fault-Tolerant Control Approach for UAV with the Control Surface Fault. *Trans. Inst. Meas. Control* **2024**, *46*, 1293–1304. [\[CrossRef\]](#)
26. Abdullah, M.; Zulfiqar, A.; Arman, J.H. An Integral Backstepping and Nonlinear Disturbance Observer-Based Sliding Mode Control for Active Fault-Tolerant Quadcopter UAVs with Simulation as Well as Hardware-in-the-Loop Experiments. *Arab. J. Sci. Eng.* **2025**, *50*, 01676. [\[CrossRef\]](#)
27. Falcón, R.; Ríos, H.; Dzul, A. Sliding-Mode-Based Fault Diagnosis and Fault-Tolerant Control for Quad-Rotors. In *Sliding-Mode Control and Variable-Structure Systems*; Oliveira, T.R., Fridman, L., Hsu, L., Eds.; Studies in Systems, Decision and Control; Springer: Cham, Switzerland, 2023; Volume 490, p. 19. [\[CrossRef\]](#)
28. Amador-Macias, M.; Hernández-Cortés, T.; Estrada-Manzo, V.; González-Sierra, J.; Tapia-Herrera, R. Actuator Fault-Tolerant Control for Mechatronic Systems and Output Regulation with Unknown Reference Signals. *Appl. Sci.* **2025**, *15*, 8551. [\[CrossRef\]](#)
29. Wang, X.; Wang, S.; Liu, J.; Wu, Y.; Sun, C. Bipartite Finite-Time Consensus of Multi-Agent Systems with Intermittent Communication via Event-Triggered Impulsive Control. *Neurocomputing* **2024**, *598*, 127970. [\[CrossRef\]](#)
30. Skogestad, S.; Postlethwaite, I. *Multivariable Feedback Control: Analysis and Design*; John Wiley & Sons: Chichester, UK, 2005.
31. Green, M.; Limebeer, D.J.N. *Linear Robust Control*; Prentice Hall: Englewood Cliffs, NJ, USA, 1995.
32. Boyd, S.; El Ghaoui, L.; Feron, E.; Balakrishnan, V. *Linear Matrix Inequalities in System and Control Theory*; SIAM: Philadelphia, PA, USA, 1994.
33. İnci, M.; Altun, Y. Disturbance Compensator Design Based on Dilated LMI for Linear Parameter-Varying Systems. *Electronics* **2024**, *13*, 3055. [\[CrossRef\]](#)
34. Borja-Jaimes, V.; Coronel-Escamilla, A.; Escobar-Jiménez, R.F.; Adam-Medina, M.; Guerrero-Ramírez, G.V.; Sánchez-Coronado, E.M.; García-Morales, J. Fractional-Order Sliding Mode Observer for Actuator Fault Estimation in a Quadrotor UAV. *Mathematics* **2024**, *12*, 1247. [\[CrossRef\]](#)
35. Menon, P.P.; Edwards, C. Robust Fault Estimation Using Relative Information in Linear Multi-Agent Networks. *IEEE Trans. Autom. Control* **2014**, *59*, 477–482. [\[CrossRef\]](#)
36. Liu, Y.; Yang, G.-H. Integrated design of fault estimation and fault-tolerant control for linear multi-agent systems using relative outputs. *Neurocomputing* **2019**, *329*, 468–475. [\[CrossRef\]](#)

Disclaimer/Publisher’s Note: The statements, opinions and data contained in all publications are solely those of the individual author(s) and contributor(s) and not of MDPI and/or the editor(s). MDPI and/or the editor(s) disclaim responsibility for any injury to people or property resulting from any ideas, methods, instructions or products referred to in the content.